OPEN ACCESS

ACTA METALLURGICA SLOVACA

2020, VOL. 26, NO. 3, 116-121

RESEARCH PAPER

ELEMENT PARTITIONING IN LOW-CARBON Si2Mn2CrMoVNb TRIP-ASSISTED STEEL IN INTERCRITICAL TEMPERATURE RANGE

Vasily Efremenko[1], Roman Kussa[1], Ivan Petryshynets[2], Kazumichi Shimizu[3], František Kromka[2], Vadim Zurnadzhy[1], Victoria Gavrilova[1]

[1] Pryazovskyi State Technical University, (PSTU) vul. Universytets'ka 7, Mariupol 87555, Ukraine

[2] Institute of Materials Research, Slovak Academy of Sciences, Watsonova 1935/47, 040 01, Kosice, Slovakia

[3] Muroran Institute of Technology, 27-1 Mizumotocho, Muroran, Hokkaido 050-8585, Japan

*Corresponding author: vgefremenko@gmail.com, Materials Science, Physics, Pryazovskyi State Technical University, (PSTU) vul. Universytets'ka 7, Mariupol 87555, Ukraine

Received: 14.05.2020
Accepted: 14.08.2020

ABSTRACT

The present paper is aimed at the study of the kinetics of Mn, Si, Cr partitioning in 0.2wt%C-Si2Mn2CrMoVNb TRIP-assisted steel under the annealing at 770 °C and 830 °C to be within the intercritical temperature range. The work was fulfilled using SEM, EDX, dilatometry, and hardness measurements. It was found that under heating a redistribution of the alloying elements between ferrite and austenite took place. Specifically, silicon partitioned to ferrite while chromium diffused to austenite with distribution coefficient values of 1.12-1.21 (K_{Si}) and 0.75-0.86 (K_{Cr}). Manganese was found to partition to a much greater extent resulting in a distribution coefficient of K_{Mn}=0.38-0.50 and 2.6 times higher concentration in austenite as compared to ferrite. As annealing temperature raised from 770 °C to 830 °C the elemental partitioning was accelerated, followed by the decrease in manganese content in austenite (by 1.44 time) and ferrite (by 1.34 time) caused by an increase in austenite volume fraction. Silicon featured uneven distribution within ferrite to be accumulated at the "martensite/ferrite" interface and near ferrite grain boundaries, while manganese was concentrated in MC carbides. The recommendation for annealing holding was formulated based on elemental partitioning kinetics.

Keywords: TRIP-assisted steel; annealing; SEM/EDX; element partitioning; ferrite; martensite

INTRODUCTION

Low carbon Mn-Si(Al) steels with TRIP effect (TRIP-assisted steels) remain attractive for researchers due to improved mechanical properties achieved under the low content of alloying elements [1-3]. They belong to the group of Advanced High Strength Steels (AHSSs) [4]. The distinguishable feature of TRIP-assisted steels is a heterogeneous multiphase structure comprising ferrite, carbide-free bainite, and retained austenite (RA) [5, 6]. According to adopted technology, TRIP-assisted steels are subjected to bainitizing heat treatment with preliminary annealing at intercritical temperature range (ITR), where carbon partitioning between ferrite and austenite takes place [1, 7, 8]. Enriched with carbon austenite retains after bainitizing, holding thus volume fraction of RA in final structure and reaches up to 10-15 vol.% [1, 9, 10]. Retained austenite is the key structural constituent of heterogeneous constructional steels due to its higher ductility and its capability toward strain-induced martensite transformation (TRIP-effect) [11, 12]. TRIP-effect results in enhancement of steel strength/ductility combination [13, 14] as well as in improvement in exploitation behaviour such as abrasive/erosive wear resistance [15-17].

A carbon partitioning between the phase constituents is a common feature of heat processing of different steel grades (TRIP-assisted steels [1, 5], Q&P-steels [18, 19], nanobainite steels [20]). During the intercritical annealing, carbon partitions between ferrite and austenite in order to reach a thermodynamic equilibrium being driven by the big difference in carbon equilibrium solubility in α-Fe and γ-Fe. A high diffusivity of carbon (as an interstitial element) under ITR makes its partitioning very fast. In addition to carbon, other (substitutional) elements (Si, Mn, Cr, etc.) could be involved in partitioning under ITR, affecting the stability of austenite to phase transformations upon bainitizing treatment or cooling [21]. This phenomenon was studied repeatedly to highlight its importance for steel transformation behaviour [22-26]. Zhang et al. [22] found that C, Mn, and Al were partitioning under ITR annealing in 0.05-0.15 wt% C -5 wt% Mn - 3 wt% Al dual-phase steels, greatly affecting austenite volume fraction and stability. Specifically, ITR annealing induced enrichment of austenite with manganese, while ferrite enriched with aluminum. The same results for manganese were reported in [23] for 6 wt% Mn - 1.4 wt% Si TRIP-assisted steel, however no partitioning of Si and Al was observed during inter-critical annealing. Lis et al. [24] found for 4 wt% Mn TRIP-steel that soft annealing at 625 °C led to the enrichment of proeutectoid cementite with Mn; besides this, a non-uniform distribution of Mn between polygonal ferrite/bainite and austenite was detected leading to increase in Mn content up to 10 wt% in martensite-austenite "islands" retained after water quenching. Lee et al. [25] showed for 6 wt% Mn steel that Mn partitioning to austenite increases the stability of retained austenite only when austenite is ultra-fine grained with grain size less than 500 nm. Luo et al. [26] demonstrated that austenite formation in 5 wt% Mn steel at the early stage of ITR annealing was controlled only by carbon diffusion. Furthermore, the newly formed 20 nm-thick austenite was formed without the Mn partitioning; however, after that manganese segregates at the γFe/αFe interface. Park et al. [27] revealed that alloying elements may partition in CMnSiAl TRIP steels not only under intercritical annealing, but under tempering at 400 °C as well.

The literature analysis allows one to conclude that investigation into elements partitioning under ITR annealing is mostly focused on medium-Mn TRIP-assisted steels and dual-phase steels alloyed by 5-7 wt% Mn. At the same time, the distribution of substitutional elements in low-Mn TRIP-assisted steel remains not well studied. Therefore the objective of the present work is to investigate the kinetics of elemental partition in low-carbon 0.2wt%C-Si2Mn2CrMoVNb TRIP-assisted steel under annealing at intercritical temperature range.

MATERIAL AND METHODS

The TRIP-assisted steel with the composition 0.20 wt% C, 1.79 wt% Si, 1.73 wt% Mn, 0.55 wt% Cr, 0.20 wt% Mo, 0.11 wt% V, 0.045 wt% Nb, 0.009 wt% S, and 0.013 wt% P was used in the present work. Steel was smelted in a 120-kg induction furnace and poured in 50 mm-diameter cast ingots which then were electro-slag remelted to produce an 80 mm diameter ingot. This ingot was subsequently forged and then rolled to a 15 mm thick strip with further soft annealing at 900 °C before machining. Then the specimens for dilatometric study (of 2 mm diameter and 20 mm length) and microscopic observation (of 3 mm x10 mm x10 mm size) were prepared. The critical points Ac_1 and Ac_3 were determined by optical dilatometer under the heating with a rate of 1.0 K/s. The isothermal heating was performed in an

electrical furnace in the air atmosphere at 770 ºC and 830 ºC. The holding durations for each temperature were 10 min, 30 min, 60 min, 120 min, and 240 min. After the holding the specimen was quenching in 20 ºC water.

The microstructure of the specimens was characterized using optical microscope (OM) Nikon 200-M and scanning electron microscope (SEM) JEOL JSM-6510. The specimens were prepared according to standard procedure and etched with the 4%-nital reagent. The volume fraction (VF) of ferrite was measured by Rosiwal lineal method [28] using the OM images of the structure. For each holding temperature five micrographs of 440 μm x 600 μm area of the same magnification were used with further averaging the results.

Phase elemental distributions were examined by the EDX method (JED-2300; JEOL). Before EDX analysis the detector was calibrated by the standard Co specimen. The average of five/seven measurements performed in the same phase was considered as phase chemical composition. Since EDX quantitative analysis of carbon in an electron microscope is difficult giving exaggerated carbon content [28], the as-obtained EDX-microprobe results were recalculated considering the total carbon content and its full carbon partitioning according to Fe-C phase diagram. The coefficient of elemental distribution between the α-phase and γ-phase was calculated as [29]

$$K_i = \frac{[i]_\alpha}{[i]_\gamma}, \qquad (1.)$$

where: $[i]_\alpha$ and $[i]_\gamma$ are the content of the i-element in the α-phase and the γ-phase respectively.

The hardness was measured using Vickers hardness tester (Future-Tech) under 30 kg load. The hardness values are an average of five/seven indentations.

RESULTS AND DISCUSSION

The selection of the regime of ITR annealing implies the data on the critical points of the steel. For this purpose, the dilatometric heating curve was analysed and the critical temperatures were found as Ac_1=760 ºC and Ac_3=930 ºC. Further, the specimens were heated from 700 ºC to 930 ºC (10 min holding) with a step of 20-30 ºC. Being heated above Ac_1 (760 ºC) the specimen acquired the ferrite/austenite structure; under the consequential water cooling the austenite transformed to martensite. Fig. 1 illustrates the effect of the temperature on ferrite volume fraction and steel hardness. Increasing the temperature between Ac_1 and Ac_3 leads to alteration of the "ferrite/martensite" ratio in favour of martensite causing the increase in hardness. The volume fraction of ferrite decreases more intensively just below Ac_1 with further slowing when approaching Ac_3. The hardness profile is inversely related to the ferrite VF profile. After holding at 930 ºC the microstructure was martensitic while the hardness reached its highest value (463 HV). From Fig. 1 the temperatures of 770 ºC and 830 ºC were selected for further investigation. The first one corresponded to the microstructure of 50 % ferrite + 50 % austenite while the latter was attributed to the microstructure of 20 % ferrite + 80 % austenite.

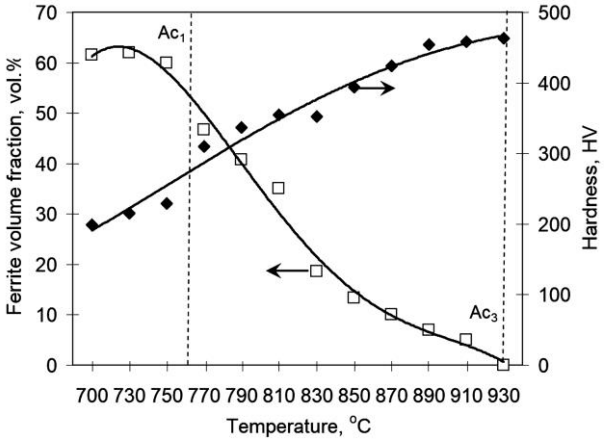

Fig. 1 Effect of the ITR temperature of ferrite volume fraction and steel hardness

Annealing at 770 ºC resulted in the microstructure consisting of ferrite and lath martensite located preferentially along the grain boundaries (Fig. 2). Grainy carbide precipitates were seen in the structure with size varied from 150 nm to 20 nm and lower. The coarse precipitates were mostly positioned in martensite areas to be associated with grain boundaries, whereas the fine nano-scaled precipitates were mostly found within the grains. Considering the presence of V and Nb in steel composition, the precipitates were assumed as a complex MC carbide ((V, Nb)C) precipitated at preliminary stages of steel manufacturing. Taking into account the size of microstructural constituents and the spatial resolution of EDX quantitative analysis (2-3 μm), the sites for the EDX-point analysis were selected in the inner part of ferrite grains or martensite areas to avoid the effect of the surrounding areas (Fig. 2, b).

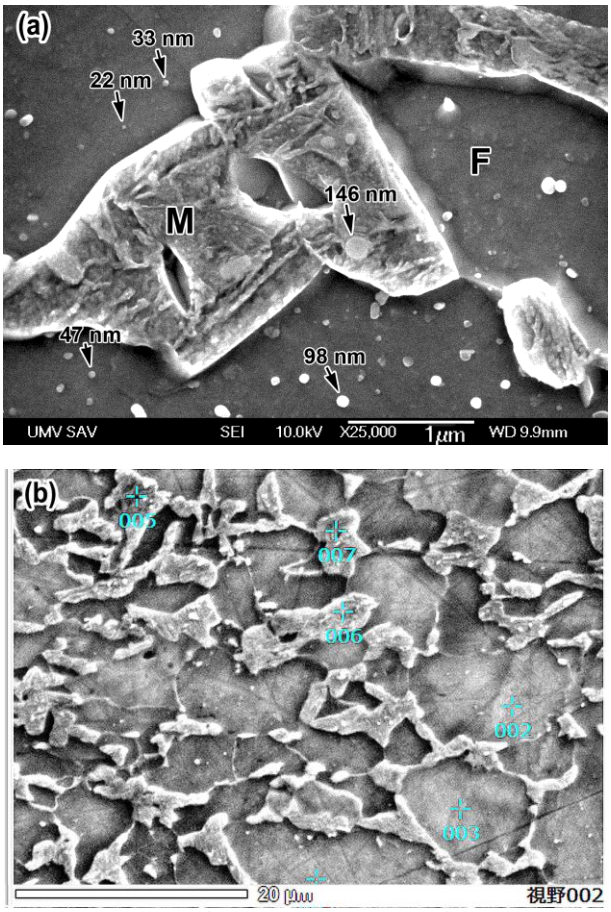

Fig. 2 The microstructure after holding at 770 ºC: (a) ferrite (F) and martensite (M) with the carbide precipitates, (b) the sites of EDX-point analyzing

As seen from Fig. 3, a, with holding time increasing the silicon content in ferrite increased from 1.83 wt% (10 min) to 2.04 wt% (60 min) with further stabilizing at this level. It was accompanied by continuous depleting of ferrite with manganese from 1.06 wt% (10 min) to 0.86 wt% (240 min). The chromium content remained stable during the entire holding duration (variation in the range of 0.58±0.03 wt%). The opposite behavior was observed for the martensitic areas (Fig. 3, b): the manganese content gradually increased from 2.12 wt% to 2.26 wt%, while silicon content decreases from 2.04 wt% with at 1.81 wt% stabilizing after 120 min holding. Also, the chromium content slightly increased in martensite from 0.68 wt% to 0.79-0.81 wt%.

The above values were extracted from the EDX-point analysis made in the core part of the ferrite/martensite areas. In contrast, the EDX observation in "scanning" modes gives more detailed information of elements' distribution. As seen from Fig. 4, manganese and silicon were unevenly distributed along the line crossing ferritic grains and martensitic areas. The Mn concentration was higher within the martensite plots (marked by the lines in Fig. 4, a). There were Mn "spikes" within martensite areas and ferrite grains associated with carbide precipitates (circled by the dotted line). Manganese content gradually decreased

from the "martensite/ferrite" interface towards the center of ferrite grain. Silicon was more unevenly distributed as compared with manganese. The mean concentration of silicon was higher in ferrite grains, however the spikes in Si concentration were revealed exactly near the "martensite/ferrite" interface. Mostly the Si-rich zones were situated in ferrite grains (Si-peaks 3, 5, and 6 in Fig. 4, a), but Si-spikes inside the martensite area were seen as well (Si-peak 1 and 2). Also, the Si-rich zone was detected at the "ferrite/ferrite" boundary (Si-peak 4). After the prolonged (240 min) holding at 770 ºC, silicon profile retained the above-described character with Si segregation in the vicinity of the "martensite/ferrite" boundary and Si-depletion inside the grains (Fig. 4, b).

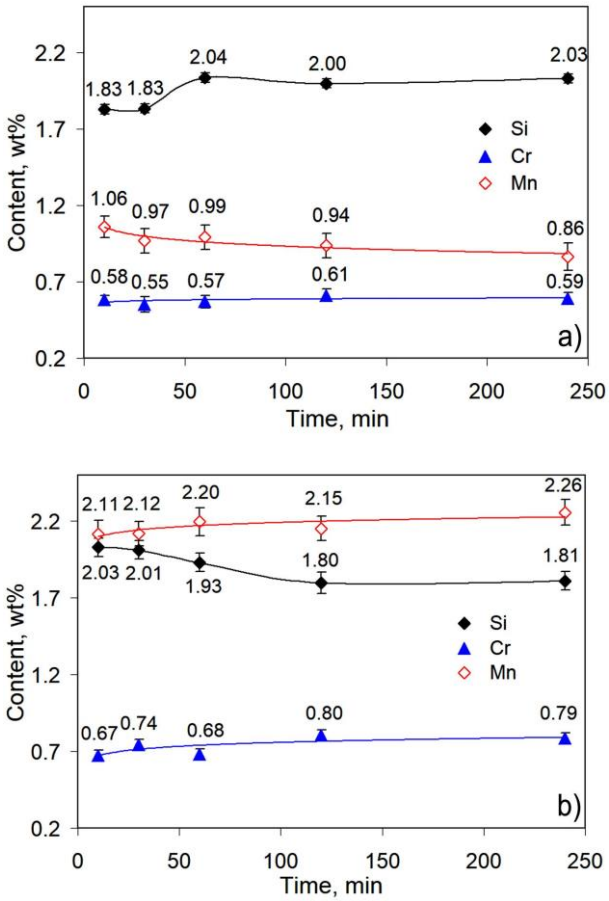

Fig. 3 Effect of holding at 770 ºC on Si, Mn, and Cr content in (a) ferrite and (b) martensite

EDX-mappings for Mn and Si are presented in Fig. 5. It is clear that the Mn-enriched areas almost completely matched the contours of martensite areas (taken from secondary electron image (SEI) in Fig. 5, a). Only two local Mn-rich areas in Fig. 5, b were not associated with martensite: a carbide aggregation (see double arrows) and the ferrite grain next to the "martensite/ferrite" interface (see the arrow). Silicon is mostly concentrated in the ferrite grains as an edging of 2-5 μm thick around the martensite areas (Fig. 5, c). The inner zones of ferrite grains are Si-depleted. Most of the silicon is concentrated in ferrite, however Si content in some martensite areas is increased (see the arrow in Fig. 5, c).

The results of EDS point analysis for the annealing at 830 ºC are presented in Fig. 6. As follows from this figure, the chemical compositions of ferrite grains and martensite areas were not significantly affected by the holding time. Only a decrease in manganese content in ferrite was noted from 0.79 wt% (10 min) to 0.59 wt% (30 min) at the early stage of the holding (Fig. 6, a). Also, silicon content in ferrite varied in a rather wide range (2.04-2.27 wt.%) caused by the smaller ferrite grains resulting in EDS-"effect" of neighbouring martensite.

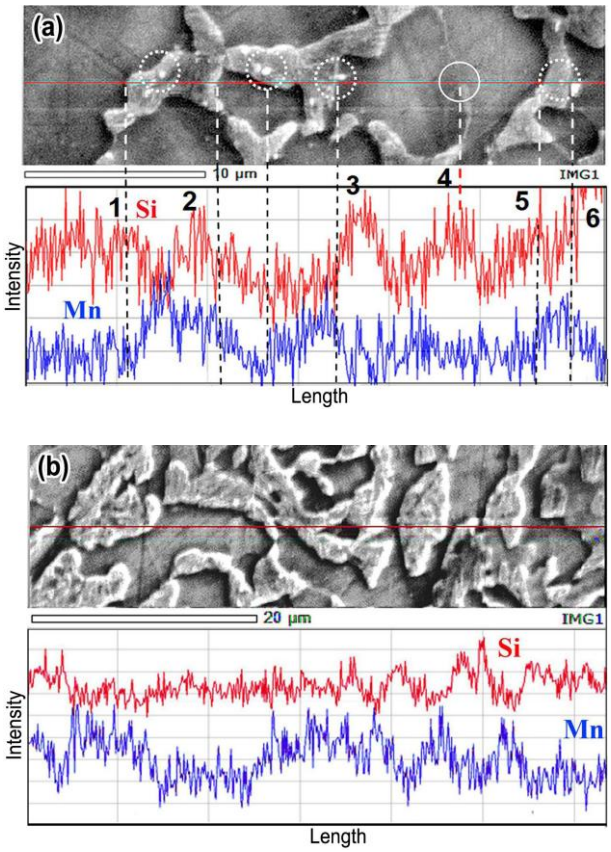

Fig. 4 SEI images of the microstructure and the profiles of Mn and Si (holding at 770 ºC for (a) 10 min and (b) 240 min)

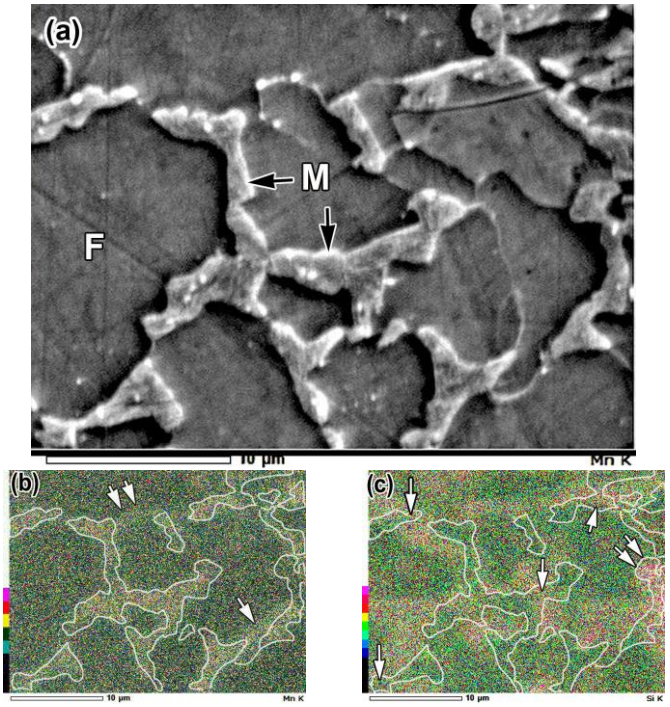

Fig. 5 (a) SEI image and the corresponding mapping of (b) Mn and (c) Si with the superimposed martensite areas contour (770 ºC, 10 min. F, M – ferrite, martensite, accordingly)

The comparison of Fig. 3 and Fig. 6 allowed one to conclude that an increase in annealing temperature from 770 ºC to 830 ºC resulted in certain variations in phase composition. Specifically, in martensite, a decrease in Mn content (from 2.20-2.26 wt% to ~1.65 wt%) and Cr content (from ~0.80 wt% to 0.66-0.70 wt%) was detected, while silicon content remained approximately at the same level. In ferrite a decrease in Mn content from ~0.90 wt% to ~0.60 wt% was revealed while Cr content almost did not change; also there was a slight increase in silicon content. An increase in annealing temperature considerably affected only the manganese content which decreased in both phases.

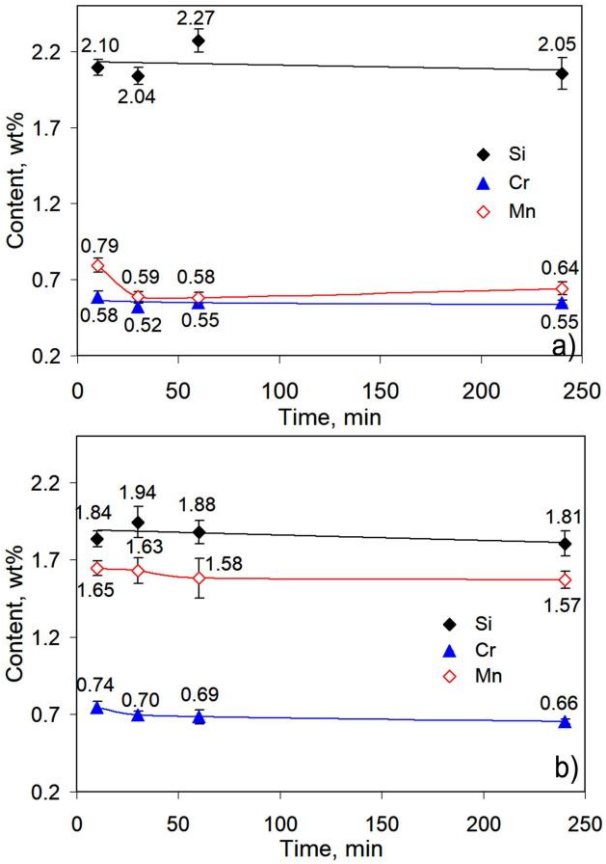

Fig. 6 Effect of holding time at 830 ºC on Si, Mn, and Cr content in (a) ferrite and (b) martensite

As follows from the mappings (Fig. 7), the holding at 830 ºC led to more pronounced partitioning the elements in different phases than at 770 ºC. Manganese was mostly concentrated in martensite, however some martensite areas were depleted with this element (shown by arrows in Fig. 7, b). The silicon distribution within ferrite grains became more homogeneous without the obvious grain-oriented segregation noted for 770 ºC (Fig. 7, c). However, EDX line-scanning still revealed the Si-spikes near the "ferrite/martensite" interface and grain boundaries although these "spikes" zones were much thinner than those at 770 ºC (about 1 μm thick).

The data obtained revealed that ITR annealing results in partitioning of Mn, Si, and Cr in the studied TRIP-assisted steel, whereas manganese partitioned to the greatest extent. At the end of 770 ºC-annealing the manganese content in austenite reached 2.26 wt.%, which is 2.6 times that of ferrite (0.86 wt%) with K_{Mn}=0.38 (Fig. 8, a). The annealing at 830 ºC led to a decrease in Mn content in austenite to 1.57 wt.% because of the increase in austenite volume fraction. With that, manganese-depleted zones appeared in martensite areas indicated by arrows in Fig. 7, b. Manganese content in ferrite decreased as well, caused by the manganese diffusivity stimulation by higher annealing temperature [30]. Thus, the distribution coefficient K_{Mn} at 830 ºC (is 0.40) remained similar to that of 770 ºC (is 0.38).

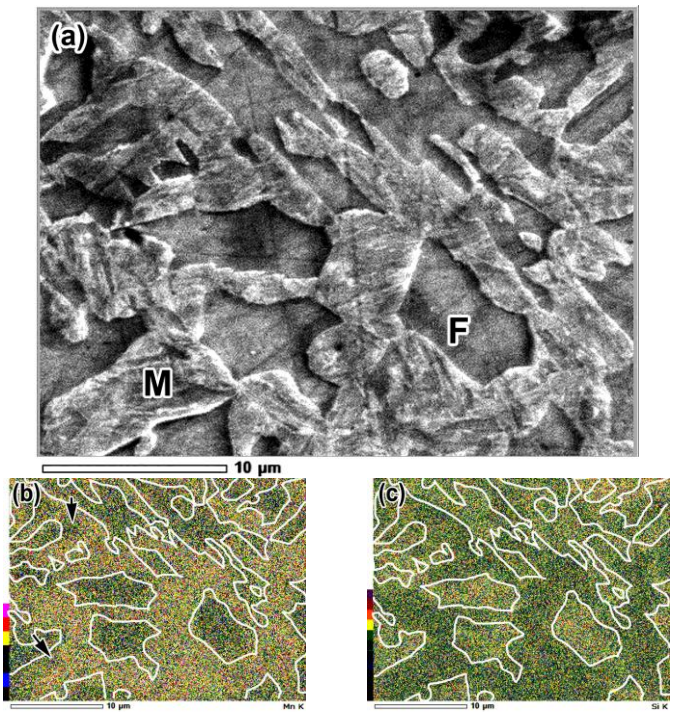

Fig. 7 (a) SEI image of microstructure and the corresponding mapping of (b) manganese and (c) silicon with the superimposed martensite contour (830 ºC for 30 min. F, M – ferrite, martensite, accordingly)

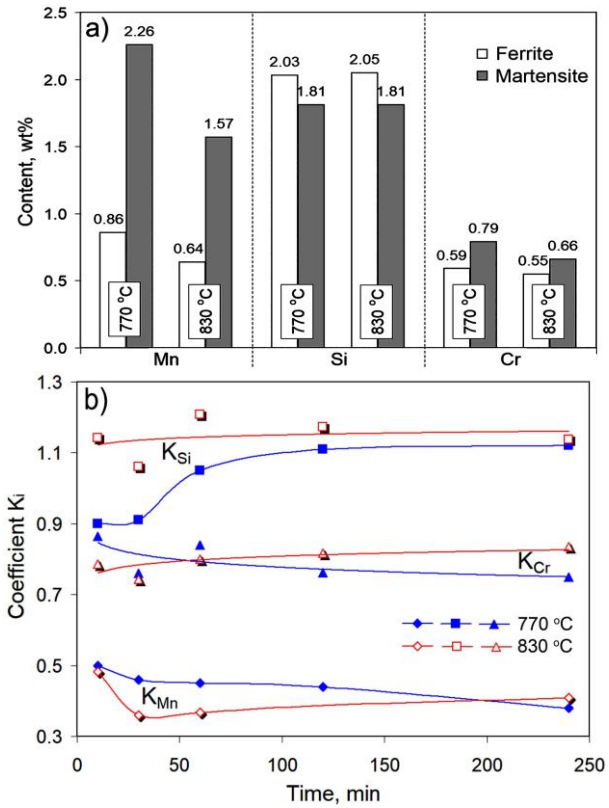

Fig. 8 (a) Phase content of Mn, Si and Cr (annealing time is 240 min) and (b) the effect of annealing time on the distribution coefficients K_{Mn}, K_{Cr}, and K_{Si}

The ferrite-stabilizing element silicon partitioned preferentially in ferrite, performing the same distribution coefficient K_{Si} (1.12-1.13) for both temperatures. Cr partitioning behavior is similar to Mn although its distribution coefficient K_{Cr} (0.75 for 770 ºC and 0.83 1.20 for 830 ºC) is much higher than that of manganese. Thus, the distribution coefficients for silicon and chromium were close to 1.0, meaning that Si and Cr are distributed approximately equally between the phases with a slight excess for the specific phase (Fig, 8, b). In contrast, the coefficient K_{Mn} (0.38-0.40) shows that. The greater part of manganese was accumulated in austenite (martensite).

The partitioning of Mn and Cr at 770 ºC proceeded with a low rate through all annealing holding (up to 240 min), which is consistent with the data of De Moor et al. [34] reported for medium-Mn "Third Generation" AHSSs subjected to intercritical annealing. However, in contrast to the observation of Luo et al. [26] and some other researchers [34, 35], we did not note the manganese segregation at the austenite/martensite interface.

The partitioning of Si at 770 ºC took place between 30-120 min holding. The distinctive feature of silicon partitioning is Si segregation at austenite/martensite interface (the same Si profile was observed by Nouri et al. [30] in dual-phase steels after annealing at 740 ºC). Noteworthy, that after 240 min holding silicon partitioning retained its uneven character while spikes of Mn concentration were associated only with carbide precipitates (Fig. 4a). The possible reason is the lower diffusivity of silicon as compared to manganese. In [30] the Si diffusion coefficient for dual-phase steels at 740 ºC was reported as $D_{\alpha Si}=3.64\cdot10^{-11}$ m^2/s for ferrite and $D_{\gamma S}=2.50\cdot10^{-15}$ m^2/s – for austenite. A big difference in D_{Si} for different phases causes an accumulation of silicon atoms at the γFe/αFe interface. In contrast, S. Sun and M. Pugh [35] found the diffusion coefficient of manganese in austenite for 0.1wt%C-2.67wt% Mn steel to be $7.12\cdot10^{-14}$ m^2/s (at 680 °C) which is an order of magnitude larger than above for silicon. Therefore manganese is evacuated faster from the boundary inward the grain, reducing its spike at the γFe/αFe interface. At 830 ºC the redistribution of manganese proceeds much faster to finish within 30 min.

Based on the above, ITR annealing at 770 ºC should not exceed 60 min. This holding time allows an increase in Mn content in austenite to stabilize it to phase transformation ensuring an increased volume fraction of retained austenite. On the other hand, the short holding will prevent the depletion of austenite by silicon. The decrease in silicon content may lead to carbide precipitation from austenite during bainitizing treatment, preventing the enrichment of austenite with carbon. This may decrease the VF of retained austenite thus negatively affecting the mechanical properties of steel [31]. ITR annealing at 830 ºC can be fulfilled with a holding of 10 min. The longer holding at 830 ºC may result in surface decarburization of the studied steel promoted by high Si content [32].

The obtained results for elemental partitioning allow predicting the volume fraction of austenite (f_{RA}) which may retain in the studied steel after bainitizing treatment:

$$f_{RA}=f_A-f_B-f_M, \quad (2.)$$

where f_A is the volume fraction of austenite at annealing temperature, f_B, is the volume fraction of bainite, f_M is the volume fraction of martensite formed after cooling from bainitizing treatment, respectively.

The volume fraction martensite can be calculated by Koistinen-Marburger equation [36]:

$$f_M=f_A-exp(-a_m\cdot(M_s-Tq)), \quad (3.)$$

where M_s is starting temperature of martensite transformation, T_q is quenching temperature, a_m is fitting parameter (0.011).

Ms temperature can be found by Andrews equation [36] based on the chemical composition (wt%) of austenite:

$$Ms=539-423C-30.4Mn-17.7Ni-12.1Cr-11.0Si-7.0Mo. \quad (4.)$$

To the end of 770 ºC-annealing (240 min) carbon content in austenite (C_A) should be almost 0.4 wt% (assuming that f_A=0.5 with full equilibrium carbon partitioning) while contents of Mn, Si and Cr are shown in Fig. 8a (molybdenum content is taken to be partitioned like chromium). For this case, M_s temperature is 270.8 ºC. According to equations (2) and (3) after the direct quenching from 770 ºC RA volume fraction should be 2.5 vol% only. However, f_{RA} can be increased in the course of bainite transformation which follows after intercritical annealing. Bainite transformation implies the rejection of carbon from bainitic ferrite into austenite causing the carbon enrichment of the latter [37]. Under silicon control the carbon is accumulated in austenite thus its concentration may reach high value, up to 1.1 wt%, as shown in [38] for 0.11 wt%C-1.5wt%Si-1.53wt%Mn steel. Presuming that bainite transformation will involve 70% of initial austenite (i.e. f_B=0.35) then carbon content in remaining austenite will increase to 1.17 wt% and M_s will decrease to minus 54.9 ºC resulting in 15 vol% of RA after final cooling.

The same calculations for 830 ºC-annealing (f_A=0.2, C_A=1.0 wt%) allow to get M_s=39.5 ºC and f_{RA}=15.6 vol% after direct quenching. Considering the high amount of carbon in austenite one can presume that this austenite will resist bainite transformation, completely retaining in the structure.

Thus, the studied steel may acquire about 15 vol.% of retained austenite as a result of elemental partitioning during intercritical annealing. This value is consistent with that previously reported in [1, 39] justifying the obtained results.

CONCLUSIONS

Based on the results obtained for 0.2wt%C-Si2Mn2CrMoVNb TRIP-assisted steel, major conclusions were drawn from this research:

1. During the annealing at 770 ºC manganese and chromium partitioned from ferrite to austenite with distribution coefficients of 0.38-0.50 and 0.75-0.86, respectively. Manganese partitioned in a greater extent resulting in manganese content in austenite to be 2.6 times that of ferrite. Silicon partitioned from austenite to ferrite with K_{Si}=0.9-1.12. An increase in annealing temperature to 830 ºC decreased the manganese content in austenite (by 1.44 times) and ferrite (by 1.34 times) whereas the content of Si and Cr remained the same to 770 ºC level.
2. Silicon is distributed unevenly within the ferrite grains, creating segregation zones near the ferrite/martensite interface or ferrite grain boundaries. As annealing temperature increased the width of these zones decreased from 2-5 μm to about 1 μm. Sharp "spikes" of manganese were associated with dispersed carbides MC.
3. At 770 ºC partitioning of Mn and Cr proceeded slowly during 240 min holding, while Si partitioning was completed after 120 min holding. At 830 ºC the elemental redistribution was finished within 30 min holding. The ITR annealing holding is recommended as 10 min for 830 ºC, and not higher than 60 min for 770 ºC.

Acknowledgments: This work is supported by Slovak Academic Information Agency (SAIA). R. Kussa and V. Zurnadzhy appreciate the support of Ministry of Science and Education of Ukraine under the project 0120U102087.

REFERENCES

1. W. Bleck, X. Guo, Y. Ma: Steel Research International, 88(10), 2019, 1700218. https://doi.org/10.1002/srin.201700218
2. H. Jirková, K. Opatová, Š. Jeníček, J. Vrtáček, L. Kučerová, P. Kurka: Acta Metallurgica Slovaca, 25(2), 2019, 101–106, http://dx.doi.org/10.12776/ams.v25i2.1267
3. Z. M. Rykavets et al.: Uspehi Fiziki Metallov, 20(4), 2019, p. 620–633. https://doi.org/10.15407/ufm.20.04.620
4. T. Nanda, V. Singh, V. Singh, A. Chakraborty, S. Sharma: Proceedings of the Institution of Mechanical Engineers, Part L: Journal of Materials: Design and Applications, 233(2), 2019, vol. 233, 209-238, https://doi.org/10.1177/1464420716664198
5. X. Tan et al.: Materials Science and Engineering: A, 771(13), 2020, 138629. https://doi.org/10.1016/j.msea.2019.138629
6. B. Fu, W.Y. Yang, Y.D. Wang, L.F. Li, Z.Q. Sun, Y. Ren: Acta Materialia, 76(1), 2014, 342-354. https://doi.org/10.1016/j.actamat.2014.05.029
7. E. Emadoddin, A. Akbarzadeh, Gh. Daneshi: Materials Characterization, 57(4-5), 2006, 408-413. https://doi.org/10.1016/j.matchar.2006.04.006
8. Z.H. Cai, H. Ding, H. Kamoutsi, G.N. Haidemenopoulos, R.D.K. Misra: Materials Science and Engineering: A, 654(27), 2016, 359-367. https://doi.org/10.1016/j.msea.2015.12.057
9. P.I. Christodoulou, A.T. Kermanidis, D. Krizan: International Journal of Fatigue, 91(Part 1), 2016, 220-231. https://doi.org/10.1016/j.ijfatigue.2016.06.004

10. B.L. Ennis et al.: International Journal of Plasticity, 88, 2017, 126-139. https://doi.org/10.1016/j.ijplas.2016.10.005
11. L.S. Malinov, I.E. Malysheva, E.S. Klimov, V.V. Kukhar, E.Yu. Balalayeva: Materials Science Forum, 945, 2019, MSF, 574-578. https://doi.org/10.4028/www.scientific.net/MSF.945.574
12. M.A. Vasylyev, B.N. Mordyuk, S.I. Sidorenko, S.M. Voloshko, A.P. Burmak: Surface and Coatings Technology. 343, 2018, 57-68. https://doi.org/10.1016/j.surfcoat.2017.11.019
13. V.I. Zurnadzhy et. al: Materials Science and Engineering: A, 745, 2019, 307–318. https://doi.org/10.1016/j.msea.2018.12.106
14. V. Kukhar, E. Balalayeva, A. Prysiazhnyi, O. Vasylevskyi, I. Marchenko: MATEC Web of Conferences, 178, 2018, 02003. https://doi.org/10.1051/matecconf/201817802003
15. A.D. Koval', V.G. Efremenko, M.N. Brykov, M.I. Andrushchenko, R.A. Kulikovskii, A.V. Efremenko: Journal of Friction and Wear, 33(1), 2012, 39-46. https://doi.org/10.3103/S1068366612010072
16. H.Y. Dong, K.M. Wu, X.L. Wang, T.P. Hou, R.Yan: Wear, 402-403, 2018, 21-29. https://doi.org/10.1016/j.wear.2018.01.009
17. V. Efremenko et al.: International Journal of Materials Research, 109(2), 2018, 147-156. https://doi.org/10.3139/146.111583
18. K. Rubešová, I. Vorel, H. Jirková, Š. Jeníček: Acta Metallurgica Slovaca, 24, 2018, 126–133. http://dx.doi.org/10.12776/ams.v24i2.1063
19. V.G. Efremenko, V.I. Zurnadzhi, Y.G. Chabak, O.V. Tsvetkova, A.V. Dzherenova: Material Science, Vol. 53, 2017, 67–75. https://doi.org/10.1007/s11003-017-0045-3
20. H. Guo, X. Feng, A. Zhao, Q. Li, M. Chai: Journal of Materials Research and Technology, 9(2), 2020, 1593–1605. https://doi:10.1016/j.jmrt.2019.11.085
21. B. Hu, H. Luo: Acta Materialia, 176(1), 2019, 250-263. https://doi.org/10.1016/j.actamat.2019.07.014
22. M. Zhang, W. Cao, H. Dong, J. Zhu: Materials Science and Engineering: A, 654, 2016, 193-202. http://dx.doi.org/10.1016/j.msea.2015.12.029
23. S.-J. Lee, S. Lee, B. C. De Cooman: Scripta Materialia, 64, 2011, p. 649–652, https://doi.org/10.1016/j.scriptamat.2010.12.012
24. J. Lis, J. Morgiel, A. Lis: Materials Chemistry and Physics, 81(2-3), 2003, 466-468, https://doi.org/10.1016/S0254-0584(03)00053-1
25. S. Lee, S.-J. Lee, B.C. De Cooman: Scripta Materialia, 65(3), 2011, 225-228, http://dx.doi.org/10.1016/j.scriptamat.2011.04.010
26. X.-N. Luo, X.-Y. Zhong, H.-W. Luo, H.-H. Zhou, C.-Y. Wang, J. Shi: Journal of Iron and Steel Research, International, 22(11), 2015, 1015-1019. https://doi.org/10.1016/S1006-706X(15)30105-9
27. H.-S. Park, J.-B. Seol, N.-S. Lim, S.-I. Kim, C.-G. Park: Materials & Design, 82, 2015, 173-180. https://doi.org/10.1016/j.matdes.2015.05.059
28. V.G. Efremenko, Yu.G. Chabak, A. Lekatou, A.E. Karantzalis, A.V. Efremenko: Metallurgical and Materials Transactions A, 47A(2), 2016, 1529-1543. https://doi.org/10.1007/s11661-016-3336-7
29. P. Rolland, V.L. Carlino, R. Vane: Microscopy and Microanalysis, 10(Suppl. 02), 2004, 964–965. https://doi.org/10.1017/S1431927604880504
30. A. Nouri, Sh. Kheirandish, H. Saghafian: Metal Sience and Heat Treatment, 59, 2018, 569–574. https://doi.org/10.1007/s11041-018-0191-8.
31. I. Spiridonova, O.V. Sukhova, A. Vashchenko: Metallofizika i Noveishie Tekhnologii, 21(2), 1999, 122-125.
32. A.D. Koval', V.G. Efremenko, M.N. Brykov, M.I. Andrushchenko, R.A. Kulikovskii, A.V. Efremenko: Journal of Friction and Wear, 33(2), 2012, 153–159. https://doi.org/10.3103/S1068366612020079
33. Y.-b. Liu, W. Zhang, Q. Tong, Q.-S. Sun: Journal of Iron and Steel Research, International, 23(12), 2016, 1316-1322. https://doi.ord/10.1016/S1006-706X(16)30194-7
34. E. De Moor, S. Kang, J. G. Speer and D. K. Matlock: Proceedings of the International Conference on Mining, Material and Metallurgical Engineering Prague, Czech Republic, 2014 Keynote Lecture II.
35. S. Sun, M. Pugh: Materials Science and Engineering: A, 276, 2000,167–174. https://doi.org/10.1016/S0921-5093(99)00261-0
36. K.W. Andrews: Journal of the Iron and Steel Institute, 203 (7), 1965, 721-727
37. V.I. Zurnadzhy et al.: Kovove Mater., 58, 2020, 129–140. https://doi.org/10.4149/km_2020_2_129
38. E. Girault, A. Mertens, J. Pascal, Y. Houbaert, B. Verlinden, J. Van Humbeeck: Scripta Materialia, 44(6), 2001, 885-892. https://doi.org/10.1016/S1359-6462(00)00697-7
39. H.-T. Jiang, W. Ding, D. Tang, W. Huang: Journal of Iron and Steel Research, International, 19(8), 2012, 29-36. https://doi.org/10.1016/S1006-706X(12)60136-8